Quantifying causal effects of green–blue–gray landscape change on urban thermal outcomes: A spatiotemporal causal machine learning analysis across city scales

Peitao Shen[1 †] Xikai Chen[1 †] Junhan Wang[1] Yinchun Fu[1,*]

1 School of Geography, South China Normal University, Guangzhou 510631, China

* Correspondence author.

† These authors contributed equally.

Corresponding author: fuyc@m.scnu.edu.cn

Abstract

Optimizing urban green–blue–gray (UGBG) landscapes has become increasingly important for mitigating surface urban heat island (SUHI) intensity under rapid urbanization. However, the causal effects of landscape pattern changes on SUHI remain poorly quantified, particularly regarding their heterogeneity among spatial configuration, urban scales, and temporal periods. This knowledge gap limits the development of adaptive and evidence-based landscape planning strategies for SUHI mitigation. To address this limitation, this study developed a causal machine learning framework to quantify the spatiotemporal causal effects of landscape pattern changes on SUHI across 836 urban core units in China. Four landscape pattern metrics representing landscape composition and configuration, including proportion of landscape (PLAND), effective mesh size (MESH), patch density (PD), and shape index (SHAPE), were evaluated for green landscapes, blue landscapes, and intergrated green–blue–gray (GBG) landscapes. A standardized counterfactual perturbation approach was applied by increasing each landscape metric by 1% relative to its original value to estimate the corresponding causal changes in SUHI intensity. The finding demonstrated that: The finding demonstrated that: (1) Increasing green landscape proportion consistently reduced SUHI across urban scales, with a 1% increase in green landscape PLAND producing approximately 1% cooling effects from small cities to megacities, and this cooling response remained stable over time. (2) Enhancing green landscape connectivity through increased MESH generated consistent cooling benefits across urban scales, with stronger cooling responses observed in small and medium cities, while these cooling benefits gradually weakened over time. (3) Patch density exhibited contrasting thermal responses between green and blue landscapes, as increased fragmentation weakened green landscape cooling but enhanced blue landscape cooling, demonstrating that similar spatial configuration changes may produce opposite thermal effect depending on landscape type. (4) Landscape shape complexity emerged as a major warming driver, with its adverse thermal effects intensifying with urban expansion and progressively amplifying over time. Increasing GBG landscape SHAPE caused stronger warming responses in larger cities, while green landscape SHAPE shifted from cooling effects in smaller cities to warming effects in large cities and megacities, indicating a scale-dependent transition of landscape complexity from beneficial to detrimental.

Overall, this study demonstrates that effective UGBG landscape optimization depends on understanding how different landscape patterns regulate SUHI across urban scale and over time. Increasing green landscape proportion provides a broadly applicable cooling pathway, improving green connectivity is particularly effective for small and medium cities, and controlling excessive landscape complexity is critical for large cities and megacities. These findings provide scale-dependent causal insights for optimizing urban green–blue–gray landscapes and advancing adaptive SUHI mitigation under future urbanization.

Keywords

Surface urban heat island; green-blue-gray landscape; Causal AI; Causal inference; Urban scale;

1 Introduction

Surface urban heat island (SUHI) refers to the thermal anomaly in which urban surface temperatures are significantly higher than those of surrounding rural areas (Liu et al., 2026; Peng et al., 2012). SUHI is primarily driven by the replacement of natural surfaces with impervious materials, anthropogenic heat emissions, and altered urban energy balances (Bowler et al., 2010; Chen et al., 2006). Under the combined pressures of global climate change and rapid urbanization, SUHI intensity continues to increase, posing substantial challenges to sustainable urban development and human well-being (Bai and Xing, 2025). Elevated SUHI intensity increases cooling demand, deteriorates thermal comfort, aggravates air-quality problems, and threatens urban ecological resilience, particularly during extreme heat events (Sadeqi and Tabari, 2024; Grimm et al., 2008; Luber and McGeehin, 2008). Therefore, developing effective and sustainable strategies for SUHI mitigation has become a critical priority in urban planning and climate adaptation.

Urban green–blue–gray (UGBG) landscapes integrate vegetated, aquatic, and built-up surfaces that jointly regulate urban thermal environments and provide important pathways for SUHI mitigation. Green and blue spaces can reduce surface temperatures through shading, evapotranspiration, evaporation, and enhanced thermal regulation, whereas gray surfaces generally exhibit higher heat absorption and storage capacity due to their impervious characteristics (Bowler et al., 2010; Gunawardena et al., 2017; Chen et al., 2019). However, under rapid urbanization, simply expanding green and blue spaces through large-scale land conversion is increasingly constrained by limited land availability and socioeconomic demands. Consequently, research attention has shifted from increasing the quantity of green and blue spaces toward optimizing the composition and spatial configuration of UGBG landscapes as an integrated urban system (Bai and Xing, 2025).

Landscape pattern theory suggests that the thermal regulation capacity of urban landscapes is strongly influenced by both compositional and configurational characteristics, including landscape proportion, connectivity, fragmentation, and shape complexity (Liu et al., 2016; Greene and Kedron, 2018). These characteristics can be quantified using landscape pattern metrics, such as proportion of landscape (PLAND), effective mesh size (MESH), patch density (PD), and shape index (SHAPE), which provide a systematic approach for evaluating how spatial organization affects urban thermal environments. Previous studies have shown that increasing green landscape proportion and improving spatial connectivity generally enhance cooling effects, whereas excessive fragmentation and irregular shapes may weaken thermal regulation by altering ecological processes and surface energy exchanges (Cui et al., 2024; Beele et al., 2024). Similarly, the cooling effects of blue landscapes depend not only on water presence but also on their spatial arrangement and configuration (Hathway and Sharples, 2012; Fei et al., 2022; Das et al., 2025). Nevertheless, the thermal consequences of UGBG landscape pattern changes may not be universal, as they can vary among different landscape types, urban scales, and temporal dynamics. Therefore, quantifying the causal effects of UGBG landscape pattern changes is essential for developing adaptive and evidence-based strategies for SUHI mitigation.

However, relationships between landscape patterns and the thermal environment are unlikely to be consistent across different urban contexts, because urban thermal responses are jointly influenced by variations in urban morphology, climatic conditions, and development trajectories (Ren et al., 2026; Zheng et al., 2026). On one hand, urban scale represents a critical dimension influencing the effectiveness of landscape pattern optimization. Cities at different development stages exhibit substantial differences in land availability, urban density, morphological structure, and anthropogenic influences, which may modify the thermal consequences of landscape pattern changes (Banerjee et al., 2022; Guo et al., 2022). Previous studies have demonstrated that the effects of urban morphological characteristics and landscape factors on thermal environments vary across urban gradients and spatial scales, indicating that landscape optimization strategies may not produce consistent benefits among cities with different spatial constraints and environmental conditions (He et al., 2024b; Zheng et al., 2026). On the other hand, relationships between landscape patterns and the thermal environment may evolve over time as urbanization processes, climatic conditions, and landscape structures continue to change. Temporal variations in urban thermal responses associated with climate dynamics and long-term urban development suggest that the effectiveness of landscape optimization strategies may not remain stable under future urban transitions (Sun, 2017; Allen et al., 2021). Therefore, identifying scale-dependent and temporally dynamic thermal responses is essential for developing adaptive and evidence-based UGBG optimization strategies.

A range of quantitative approaches have been developed to investigate the relationships between UGBG landscape patterns and SUHI intensity. Traditional statistical methods, including correlation analysis, regression models, and spatial statistical approaches, have provided important insights into UGBG landscape and SUHI. However, these methods generally rely on predefined functional assumptions and are limited in capturing nonlinear interactions and heterogeneous responses across urban contexts (Zheng et al., 2026; An et al., 2025). Machine learning approaches, particularly tree-based ensemble models such as random forests and XGBoost, have further improved the ability to identify nonlinear relationships, important landscape drivers, and potential thresholds (Breiman, 2001; Chen and Guestrin, 2016; He et al., 2024b; Qu et al., 2025). Nevertheless, predictive performance and variable importance cannot directly reveal the causal effects of landscape interventions, as observed associations may be confounded by factors such as urban morphology, climate conditions, and human activities. Causal machine learning provides a promising framework to address these limitations by integrating causal inference with flexible machine-learning algorithms. Based on the potential outcomes framework, it estimates counterfactual responses under alternative landscape intervention scenarios and enables the identification of heterogeneous treatment effects while accounting for nonlinear relationships and confounding structures (Rubin, 2005; Pearl, 2000; Chernozhukov et al., 2018; Wager and Athey, 2018; Athey et al., 2019). Therefore, causal machine learning offers an appropriate approach for quantifying the heterogeneous effects of UGBG landscape pattern changes on SUHI intensity across different urban contexts.

Based on the above scientific understanding and methodological challenges, this study develops a causal AI framework to quantify the spatiotemporal causal effects of UGBG landscape pattern changes on SUHI. China provides an ideal empirical context because rapid urbanization has substantially reshaped urban landscape structures, while its diverse urban systems encompass cities with different development stages, spatial scales, and landscape transformation trajectories. The availability of long-term remote sensing observations across a large number of urban areas further enables the investigation of heterogeneous causal effects over space and time. Using 836 Chinese urban core areas as empirical cases, this study investigates how landscape interventions influence SUHI intensity across different urban scales and temporal periods. Specifically, this study aims to: (1) characterize the spatiotemporal dynamics of SUHI intensity and UGBG landscape patterns in Chinese cities; (2) quantify the causal effects of key UGBG landscape pattern indicators on SUHI intensity under counterfactual intervention scenarios; and (3) reveal the spatial and temporal heterogeneity of these causal effects across different urban scales. By moving beyond correlation-based and predictive analyses, this study provides a causal understanding of how UGBG landscape optimization can contribute to adaptive and evidence-based SUHI mitigation strategies.

2 Material and methods

2.1 Study framework

As shown in Fig. 1, this study establishes a four-step analytical framework to investigate how UGBG landscape pattern changes influence SUHI intensity across different urban scales. Step 1 involves data collection and preprocessing, including the integration of SUHI datasets, land use/land cover data, climate variables, and human activity data. Step 2 characterizes the spatiotemporal dynamics of SUHI intensity and UGBG landscape patterns across 836 Chinese urban core areas from 2001 to 2020. Specifically, green, blue, and integrated green–blue–gray (UGBG) landscape patterns are identified from land use/land cover data, and landscape pattern indicators are calculated at both landscape and class levels. The Mann–Kendall (M-K) trend test and Sen's slope estimator are then applied to quantify temporal trends and the magnitude of changes in SUHI intensity and landscape pattern characteristics. Step 3 applies causal forest models to estimate the causal effects of UGBG landscape pattern interventions on SUHI intensity under counterfactual scenarios. Step 4 further investigates the heterogeneity of these causal effects by examining variations across different city scales, landscape indicators, and temporal periods. This framework integrates spatiotemporal analysis with causal inference, providing a systematic approach for understanding the thermal consequences of UGBG landscape optimization and supporting evidence-based urban climate adaptation strategies.

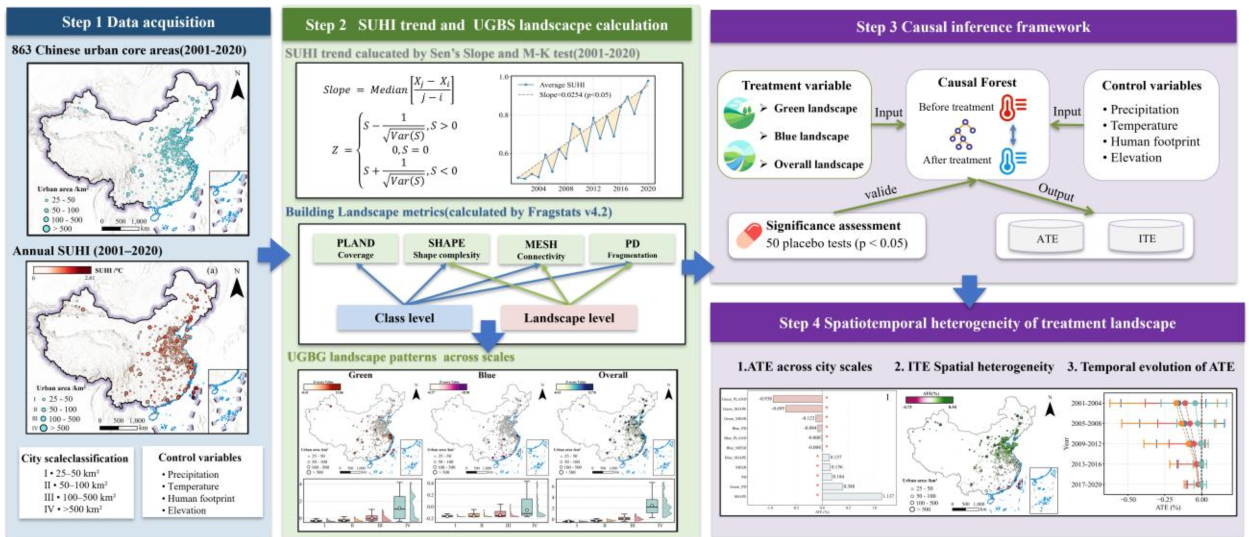

Fig. 1. Research framework of this study.

2.2 Study area

This study focuses on 836 urban core areas across China. China is a particularly important research region due to its rapid and extensive hyper-urbanization, which generates diverse SUHI patterns across different climatic and morphological settings, ranging from the cold-temperate Northeast to the humid subtropical South and the arid Northwest (Du et al., 2021; Beck et al., 2020). Using the Global Urban Boundary (GUB) dataset (Li et al., 2020), we selected core built-up areas exceeding 25 km², with the 2018 urban boundary as the spatial reference for the 2001–2020 study period. The term "urban area" here refers to both individual cities and larger urban clusters because the GUB data preserves spatial continuity. To distinguish cities of different scales, we define small cities as those with built-up areas between 25 and 50 km², medium cities between 50 and 100 km², large cities between 100 and 500 km², and megacities over 500 km². The use of a single year (2018) as the spatial reference ensures that the urban core area is consistent over the 20-year study period, so that changes in UGBG landscape pattern reflect real landscape transitions rather than boundary redefinitions. Throughout the paper, for ease of visualization, the four scale groups are also labelled I, II, III and IV in figures and tables.

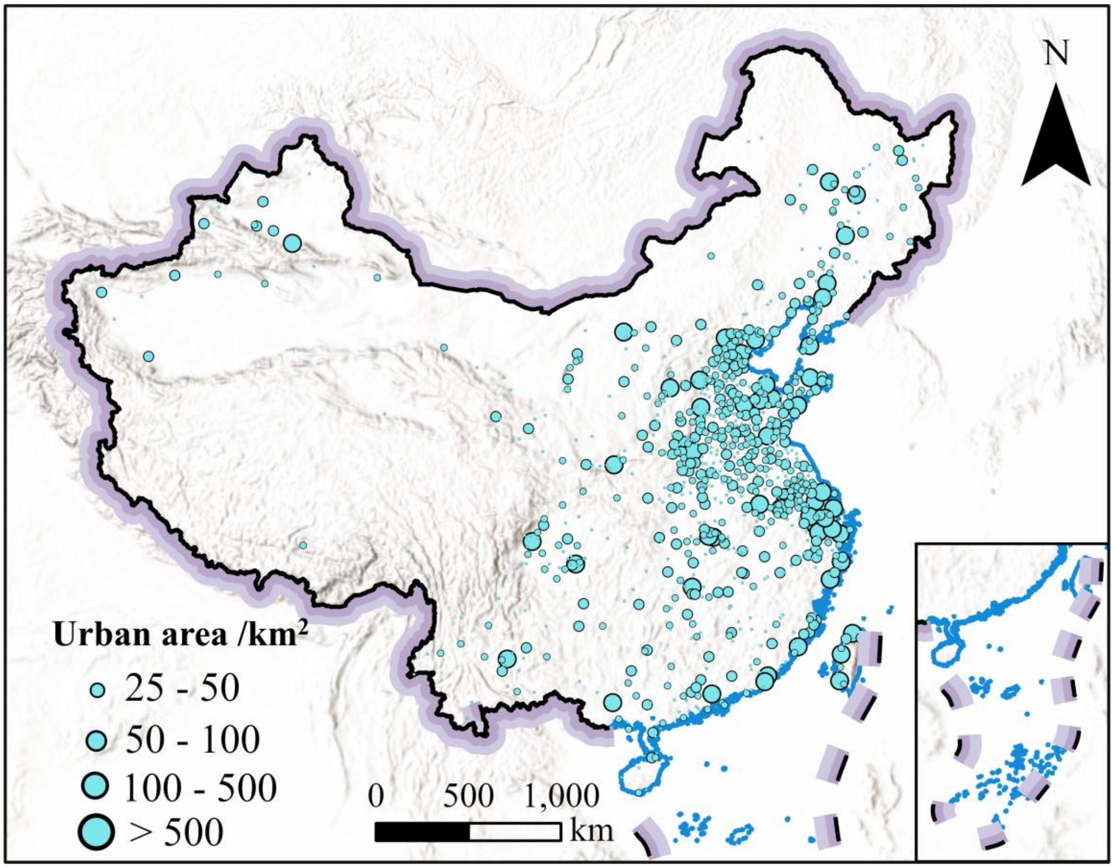

Fig. 2. Study area and spatial distribution of cities across different scales.

2.3 Data sources and preprocessing

This study utilizes land surface temperature and land cover data to investigate the causal effects of UGBG landscape pattern changes on SUHI intensity, while precipitation, air temperature, human activity, and elevation data are incorporated as control variables to account for potential confounding effects. These multiple datasets were collected from:

(1) SUHII data from the AMOD UHII dataset (Yang et al., 2024; https://doi.org/10.6084/m9.figshare.24821538), derived by integrating the global seamless all-sky clear-sky land surface temperature product with multi-source information at monthly resolution, aggregated to annual scale for 2001–2020;

(2) Land use/ land cover data from the China annual 30-meter resolution land cover dataset(Yang et al., 2023; https://zenodo.org/records/15853565), which was reclassified into three categories: blue space (water bodies, wetlands), green space (cropland, forest, shrub, grassland), and gray space (impervious land);

(3) Human activity data from the Global human footprint dataset(Mu et al., 2022; https://figshare.com/articles/figure/An_annual_global_terrestrial_Human_Footprint_dataset_from_2000_to_2018/16571064). This dataset present the human pressure of urbanlization and economic development.

(4) Annual precipitation and temperature from TerraClimate dataset and the elevation dataset from National Aeronautics and Space Administration. Those were ultilize as control varible in machine learning modelling and causal inference. Those datasets were extracted in google earth engine(https://developers.google.com/earth-engine/datasets?hl)

2.4 Methods

2.4.1 Spatiotemporal dynamic analysis of SUHI

This study divides different scale city and employs the Mann-Kendall(M-K) trend test and Sen's slope method to analyze the spatiotemporal variation trends of SUHI. The M-K test is a non-parametric approach that does not require data to follow a normal distribution and effectively mitigates interference from outliers, making it widely applicable in analyzing time-series data in vegetation, climate, and other related fields. The SUHI spatiotemporal dynamic is calculated based on formulas (1-4):

$$S = \Sigma_{i=1}^{n} \Sigma_{j=i+1}^{n} sgn\left(X_j - X_i\right) \tag{1}$$

$$sgn\left(X_j - X_i\right) = \left(1, X_j - X_i > 0;\ 0, X_j - X_i = 0;\ -1, X_j - X_i < 0\right) \tag{2}$$

$$Z = \left(S - \frac{1}{\sqrt{Var(S)}}, S > 0;\ 0, S = 0;\ S + \frac{1}{\sqrt{Var(S)}}, S < 0\right) \tag{3}$$

$$Slope = Median\left[\frac{X_j - X_i}{j - i}\right], 0 \leq i < j \leq n \tag{4}$$

the S test first computes the sum of sign differences across the time series, then the Z value is obtained after variance correction. When $|Z| > Z_{1-\frac{p}{2}}$, the trend is considered statistically significant; $Z > 0$ indicates an increasing trend, while $Z < 0$ indicates a decreasing trend. Sen's slope method estimates the trend magnitude by calculating the median of change rates between any two points, demonstrating strong robustness against outliers and providing a more accurate representation of the true variation characteristics in long-term time-series data.

2.4.2 Landscape indicator calculation

Feature variables include green, blue, and integrated green–blue–gray (GBG) landscape pattern indicators, together ywith four control variables. Four landscape metrics are selected to characterize the compositional and configurational characteristics of GBG landscapes (Table 1), including effective mesh size (MESH), patch density (PD), percentage of landscape (PLAND), and mean shape index (SHAPE). These metrics are calculated separately for green landscapes, blue landscapes, and integrated GBG landscapes, resulting in 11 landscape pattern variables. Specifically, green landscape indicators are denoted as G-MESH, G-PD, G-PLAND, and G-SHAPE; blue landscape indicators are denoted as B-MESH, B-PD, B-PLAND, and B-SHAPE; and integrated GBG landscape indicators are denoted as GBG-MESH, GBG-PD, GBG-PLAND, and GBG-SHAPE, respectively. MESH represents the effective connectedness, PD quantifies landscape fragmentation by measuring the number of patches per unit area, PLAND reflects the proportional coverage of landscape components, and SHAPE characterizes patch shape complexity and potential edge effects (Bowler et al., 2010; Qu et al., 2025). All landscape metrics are calculated using Fragstats v4.2 based on annual 30-m land cover maps and subsequently aggregated to the urban core area level. Multicollinearity among explanatory variables is assessed using the variance inflation factor(VIF) in SPSS v26.0. All VIF values are below 10, indicating that multicollinearity does not substantially affect the subsequent modelling. The detailed VIF results are provided in the Supplementary Material Table1.

Table 1

Indicators of control variables and landscape factors.

Category	Indicator	Abbreviation	Description
Control variable	Human Footprint	/	Cumulative human impact integrating population density, infrastructure, and land-use change.
	Precipitation	/	Mean annual precipitation representing water availability and climatic conditions.
	Temperature	/	Mean annual temperature representing thermal condition and energy availability.
	Elevation	/	Digital elevation model representing topographic condition and altitude.
Landscape metric	Effective mesh size	MESH	Effective mesh size of patches, measuring effective patch connectivity.
	Patch density	PD	Density of patches per unit area, measuring landscape fragmentation.
	Percentage of landscape	PLAND	Proportion of the landscape occupied by the corresponding patch type, reflecting coverage.
	Mean shape index	SHAPE	Mean shape index of patches, measuring patch shape complexity and edge effect.

2.4.3 Causal machine learning algorithm based on causal forest

To estimate the causal effects of UGBG landscape pattern interventions on SUHI intensity, this study develops a causal inference framework based on Causal Forest with orthogonalization and cross-fitting strategies derived from the double machine learning framework (Chernozhukov et al., 2018; Ahrens et al., 2025). These procedures reduce the bias caused by high-dimensional nuisance functions and allow flexible machine-learning models to estimate treatment and outcome relationships while maintaining valid causal inference. Causal forest is a non-parametric ensemble approach designed to estimate heterogeneous treatment effects by partitioning observations according to differences in treatment responses (Wager and Athey, 2018; Athey et al., 2019). In this framework, the average treatment effect (ATE) represents the expected change in SUHI intensity resulting from a specific landscape pattern intervention across all urban areas, whereas the individual treatment effect (ITE) describes the corresponding causal effect for each individual urban unit, enabling the identification of spatial and temporal heterogeneity.

In this study, each landscape indicator is considered as a continuous treatment variable, and the counterfactual treatment level is defined as a 1% increase relative to the observed value in the original data space. The treatment variables are then standardized separately before and after the intervention to ensure comparability across indicators. The causal effect of each intervention is estimated by comparing the predicted SUHI outcomes under observed and counterfactual treatment scenarios while controlling for potential confounding factors, including climatic conditions, topographic characteristics, and human activity intensity.

$$T_1 = T_0 * 1.01 \tag{5}$$

$$\tau(x) = E[Y_i | T_i = T_1, X_i = x] - E[Y_i | T_i = T_0, X_i = x] \tag{6}$$

$$\widehat{\tau(x)} = \frac{1}{B}\sum_{b=1}^{B} \widehat{\tau_b(x)} \tag{7}$$

Where T_0 is the standardized treatment value, and T_1 represents the counterfactual treatment level of adding 0.01 for itself. Y_i is the SUHI outcome variable, T_i is the landscape pattern change treatment variable, and X_i is the vector of control variables (including climate, topography, and human activities). The counterfactual scenario is defined as the expected outcome if the landscape pattern change treatment were set to a different value, while holding all other variables constant. As shown in the equation, where B is the number of trees and each $\widehat{\tau_b(x)}$ is an honest subsample estimate. To examine the statistical significance of each treatment variable, we conducted 50 placebo tests for each by randomly shuffling the treatment variable, with $p < 0.05$ indicating statistical significance

3 Results

3.1 Spatiotemporal dynamics of SUHI

Fig. 3 shows the spatiotemporal distribution of SUHI in Chinese cities from 2001 to 2020. Spatially (Fig. 3a), SUHI exhibits clear regional differentiation: cities in eastern coastal regions generally show higher SUHI intensity, whereas cities in central, western, and southern mountainous regions display relatively lower SUHI. From the perspective of temporal trends across city scales (Fig. 3b–f), the SUHI warming rate accelerates significantly with urban scale. The Sen's slope rises from 0.023 yr^{-1} in small cities to 0.038 yr^{-1} in megacities, an increase of approximately 1.6 times. All four scale groups pass the M-K test at the $p < 1 \times 10^{-6}$ level, indicating that the observed warming trends are highly statistically significant. Specifically, the initial SUHI value is 0.43 in small cities and 0.78 in megacities; the overall mean SUHI increases from 0.47 to 0.98 over the 20-year period, beyond a doubling (+107.6%). When measured in absolute terms, the total SUHI increase exceeds 1.5 °C in megacities and 1.0 °C in large cities, underscoring the severity of the SUHI problem at the largest scale. The smaller relative slope in small cities is consistent with the fact that small urban cores are more strongly modulated by their rural surroundings, while the larger absolute slope in megacities reflects the compounded effects of large impervious surface fractions, high building volume, and strong anthropogenic heat fluxes. Together, SUHI intensifies in megacities by roughly 1.6 times faster than in small cities.

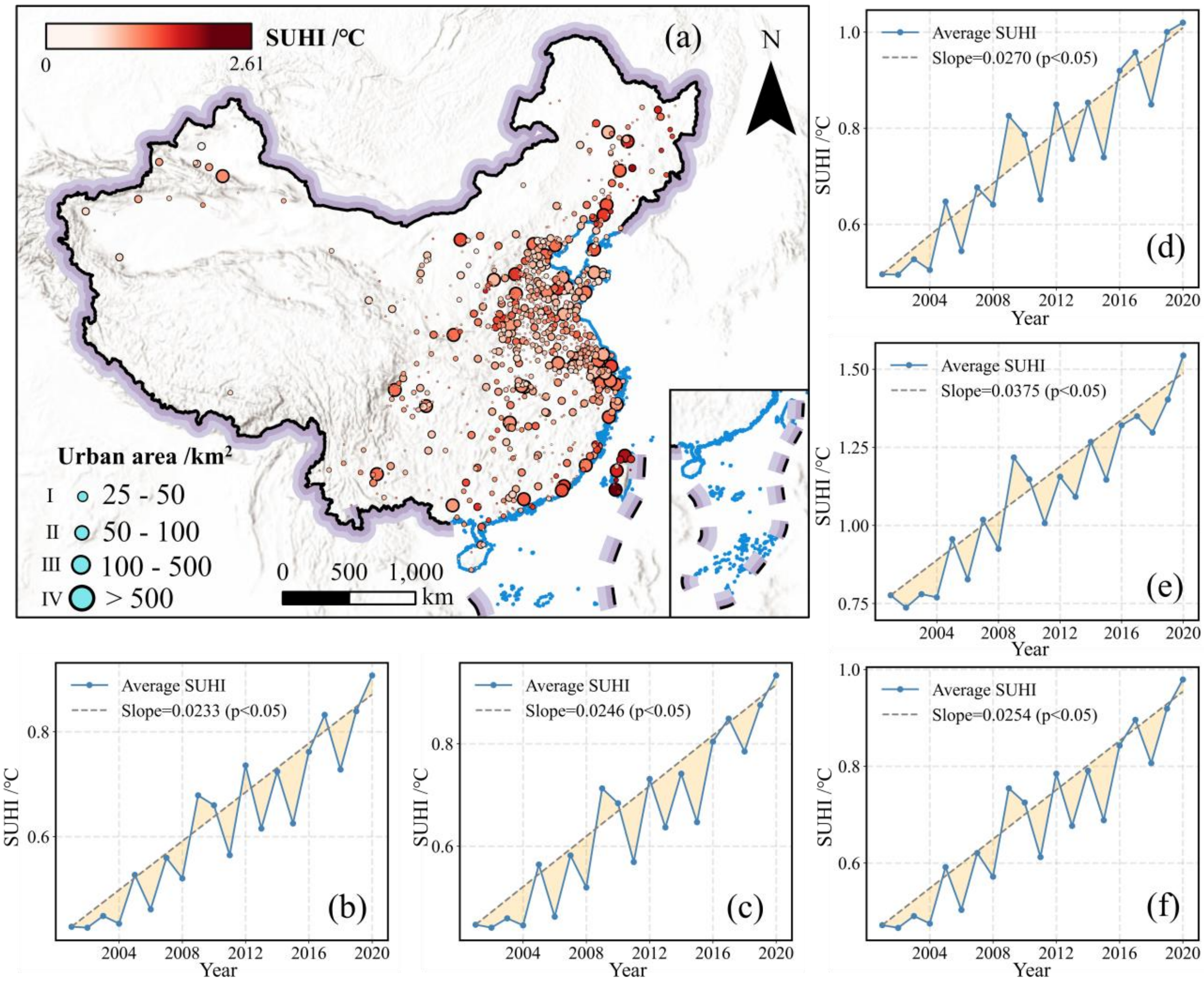

Fig. 3. Spatiotemporal distribution of SUHI in China and variation trends across urban scales. (a) The spatial distribution of SUHI in China (b)-(f) The slope and tendency of SUHI change across 2001-2020 in small cities, medium cities, large cities, and megacities.

3.2 Spatial differentiation of UGBG landscape patterns across urban scales

Fig. 4 illustrates the differentiated distribution of UGBG landscape patterns across urban scales and geographic regions. GBG-MESH shows higher values in megacities than in the other three urban-scale groups, whereas the values in small, medium, and large cities exhibit relatively similar distributions. G-MESH also presents higher values in megacities, with clear differences among urban-scale groups. G-PD and G-SHAPE display the widest variations in small cities, while their distributions are relatively concentrated in larger cities. G-SHAPE generally shows lower values in megacities than in the other urban-scale groups, indicating differences in green landscape configuration among cities with different development scales. G-PLAND exhibits higher values in western China, whereas other regions show relatively diverse distributions.

Spatially, UGBG landscape indicators display evident regional variations. Western cities show relatively lower landscape proportion and greater variability across landscape metrics, while central cities present comparatively moderate distributions. Northeastern cities exhibit lower G-PD and G-MESH values than most other regions. Southern and western regions show broader variations in fragmentation-related indicators, particularly PD-based metrics.

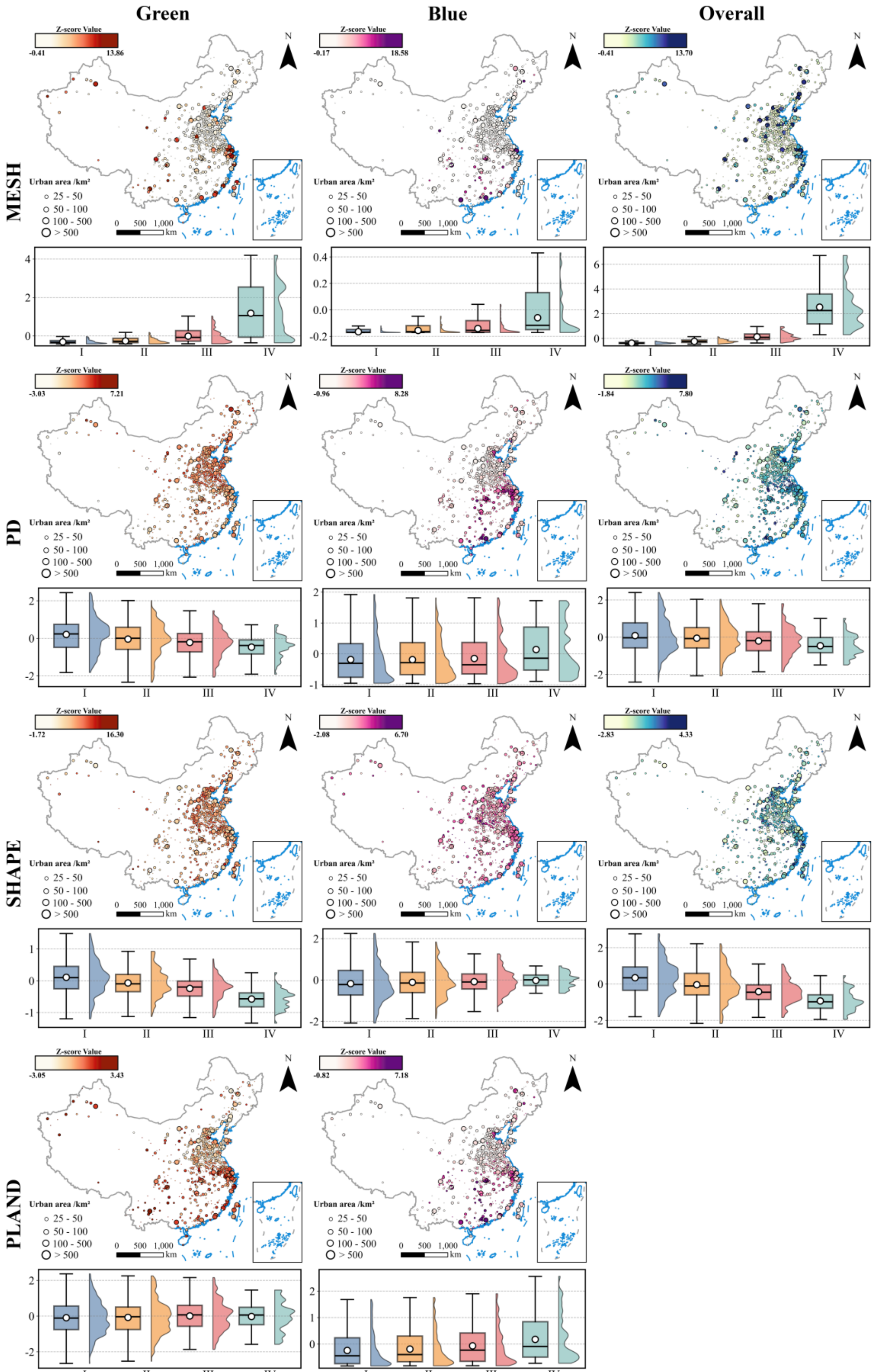
Green
Blue
Overall
MESH
PD
SHAPE
PLAND
Z-score Value
Urban area /km²
25 - 50
50 - 100
100 - 500
> 500
0 500 1,000 km
N
I
II
III
IV

Fig. 4. Spatial distribution and comparison of standardized UGBG landscape pattern data across different urban scales. Green and Blue indicate the single landscape pattern of green space and blue space; Overall indicating the integrated UGBG landscape pattern. I, II, III, and IV correspond to small cities, medium cities, large cities, and megacities, respectively.

3.3 Effects of UGBG landscape patterns change on SUHI

3.3.1 Causal inference of UGBG landscape change effects on SUHI

The causal inference results (Figs. 5 and 6) show that 43 of 44 treatment variables produce statistically significant effects on SUHI intensity and pass 50 placebo tests ($p < 0.05$).

For MESH-related indicators, G-MESH, B-MESH, and GBG-MESH show relatively limited variations in causal effects across urban scales. The ATE values of MESH-related indicators remain within a relatively narrow range among small cities, medium cities, large cities, and megacities (Fig. 5). Similar patterns are observed across geographic regions, with relatively small differences among regional groups (Fig. 6).

For SHAPE-related indicators, stronger scale-dependent variations are observed. GBG-SHAPE shows positive ATE values across all urban scales, increasing from +1.14% in small cities to +7.08% in megacities. G-SHAPE presents negative ATE values in small and medium cities (−0.70% and −1.09%), but positive values in large cities and megacities (+0.55% and +5.57%). B-SHAPE shows positive ATE values in small, medium, and large cities (+0.14%, +0.45%, and +0.57%), while a negative value is observed in megacities (−0.60%). Spatially, SHAPE-related indicators display larger regional differences than other metric groups, with variations among regions particularly evident in megacities and small cities.

For PD-related indicators, G-PD and B-PD exhibit relatively moderate causal effects across urban scales. The differences in ATE values among small cities, medium cities, large cities, and megacities remain relatively limited, and the regional distributions show comparatively smaller variations than SHAPE-related indicators.

For PLAND-related indicators, G-PLAND shows negative ATE values across all urban scales, with values of −0.94% for small cities, −1.01% for medium cities, −1.09% for large cities, and −0.91% for megacities. The difference among urban-scale groups is within 0.18 percentage points.

B-PLAND also exhibits negative ATE values across all scales, ranging from −0.01% to −0.16%. Compared with other indicators, PLAND-related effects show relatively stable patterns across urban scales and regions.

Overall, the causal effects of UGBG landscape pattern indicators vary among metric types, urban scales, and geographic regions. MESH and PD indicators show relatively smaller variations, whereas SHAPE indicators exhibit stronger differences across urban scales and regions.

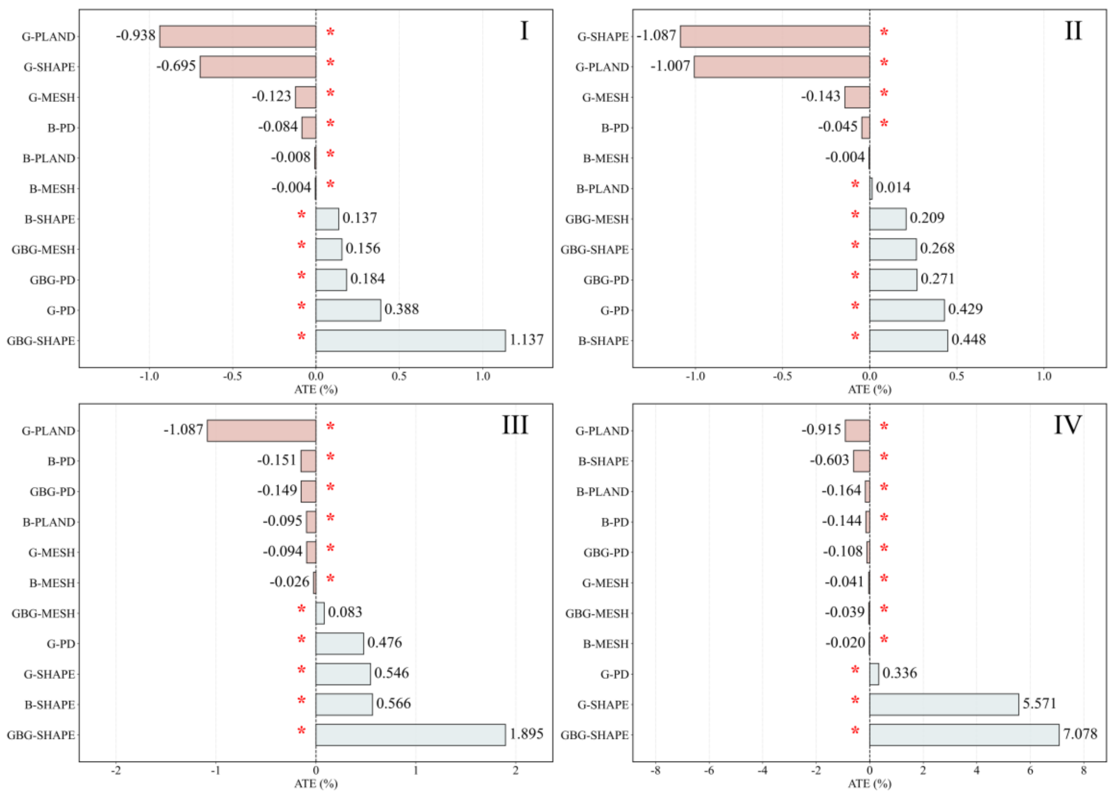

Fig. 5. Average treatment effects of UGBG landscape indicators on SUHI. I, II, III, and IV correspond to small cities, medium cities, large cities, and megacities, respectively.

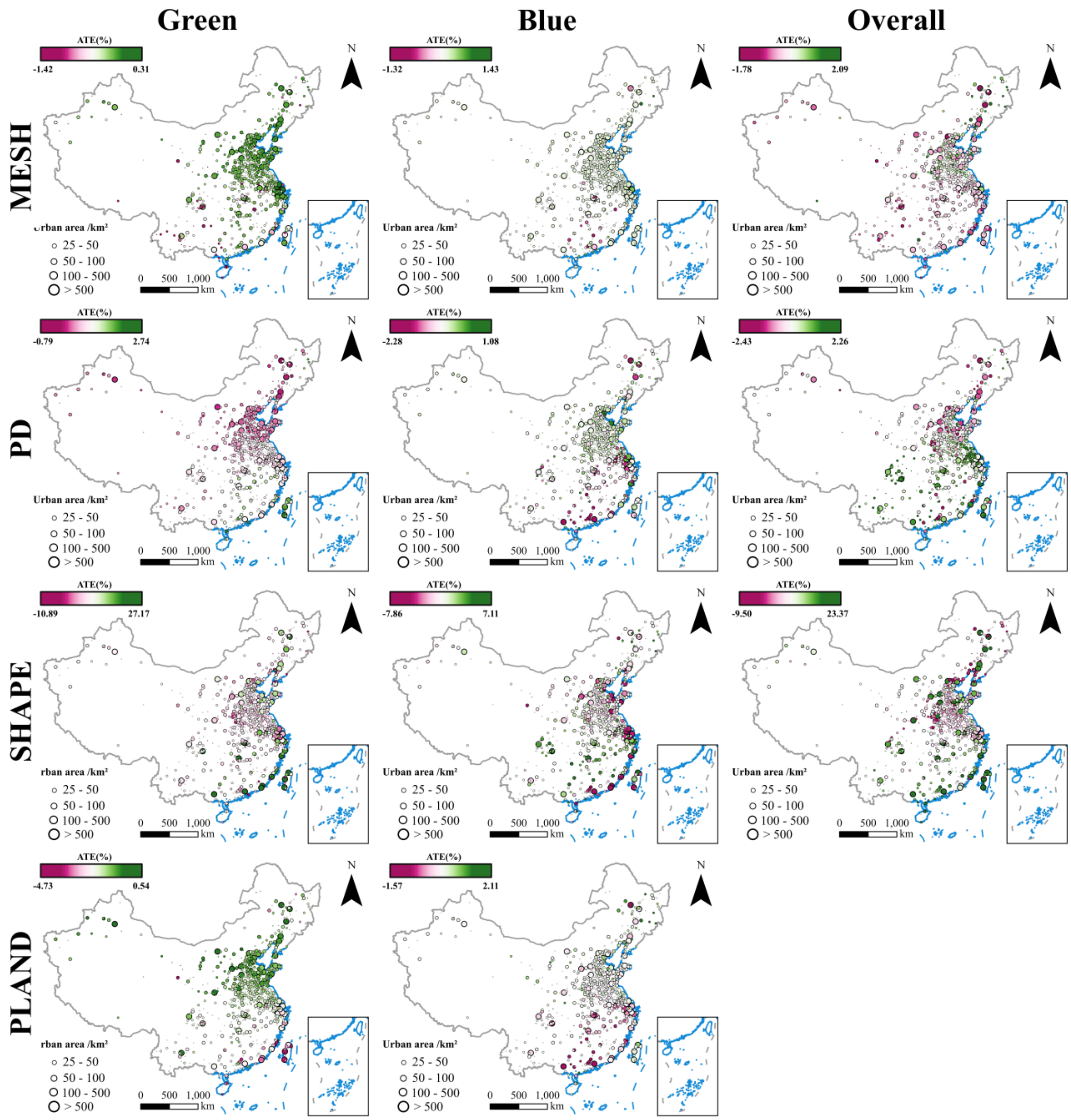

Fig. 6. Spatial distribution of causal effects across regions. Green and Blue indicate the single landscape pattern of green space and blue space; Overall indicating the integrated UGBG landscape pattern. I, II, III, and IV correspond to small cities, medium cities, large cities, and megacities, respectively.

3.3.2 Temporal changes in UGBG landscape change effects on SUHI

Based on the five-year aggregated periods from 2001 to 2020 (Fig. 7), the temporal variations of ATE values for UGBG landscape pattern interventions were examined across different urban scales. The results show that the magnitude of causal effects varies among landscape indicators and urban-scale groups over time.

For MESH-related indicators, G-MESH exhibits negative ATE values across all urban scales during the study period. However, the absolute magnitude of G-MESH effects gradually decreases over time, indicating a weakening cooling effect throughout the study period.

For SHAPE-related indicators, GBG-SHAPE and G-SHAPE show the largest temporal variations among all landscape metrics. The ATE values of GBG-SHAPE in megacities increase from +5.11% in 2001–2004 to +7.87% in 2017–2020. G-SHAPE shows different temporal trajectories among urban scales, with negative ATE values in small and medium cities and positive ATE values in large cities and megacities throughout different periods. The differences in ATE values among urban-scale groups become larger over time.

For PD-related indicators, the temporal variations of G-PD and B-PD remain relatively limited across different periods and urban scales. The ATE values show comparatively stable patterns, with no substantial changes in effect magnitude.

For PLAND-related indicators, G-PLAND maintains negative ATE values throughout all periods and urban scales. The values remain within a relatively narrow range (−0.88% to −0.99%), showing limited temporal variation. B-PLAND also presents relatively stable temporal patterns across the study period.

Overall, the temporal analysis demonstrates that the causal effects of UGBG landscape pattern indicators vary across different periods, urban scales, and metric types. SHAPE-related indicators exhibit stronger temporal fluctuations, whereas PLAND-related indicators show relatively stable temporal patterns.

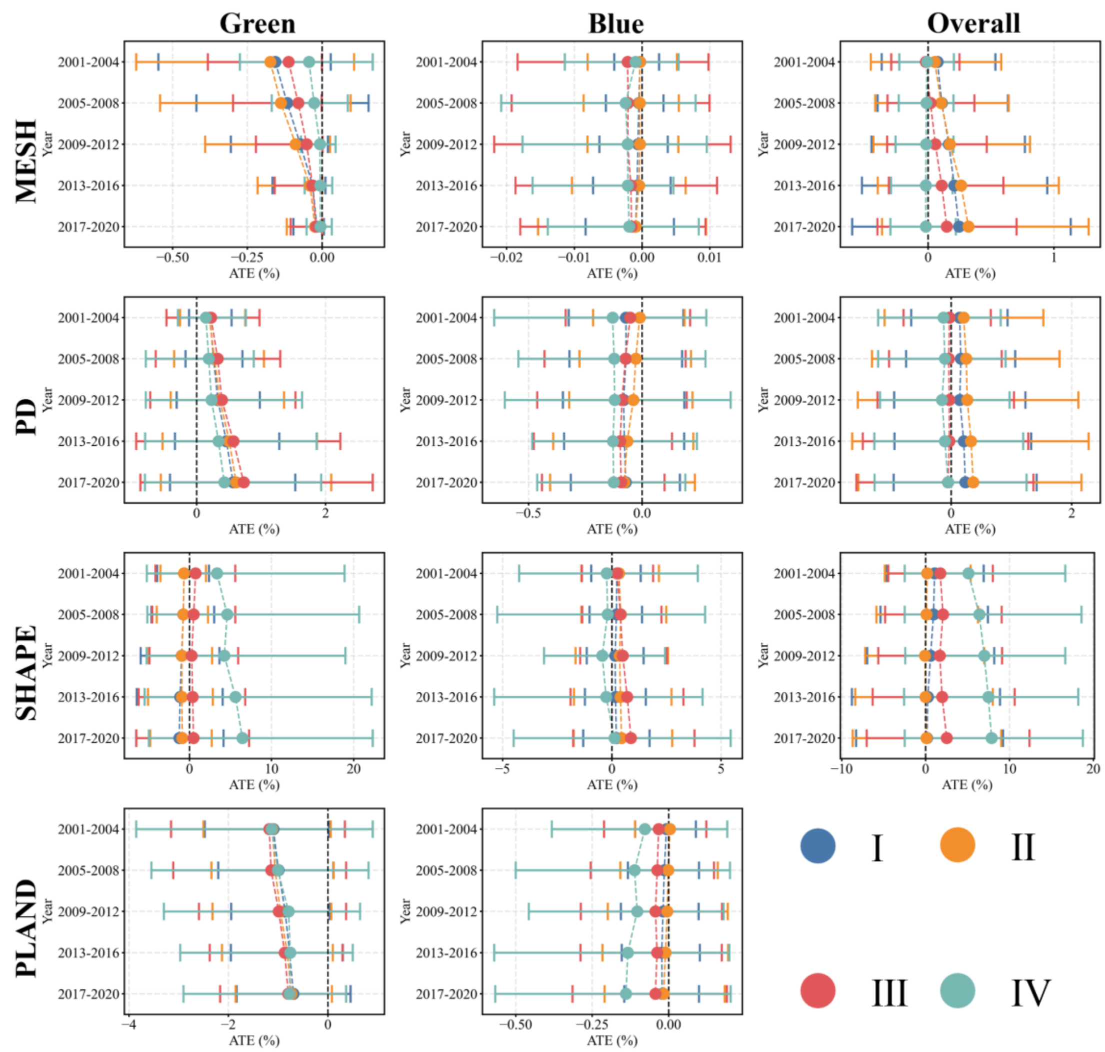

Fig. 7. Temporal change of average treatment effects in five period. Green and Blue indicate the single landscape pattern of green space and blue space; Overall indicating the integrated UGBG landscape pattern. I, II, III, and IV correspond to small cities, medium cities, large cities, and megacities, respectively.

4 Discussion

4.1 Understanding scale-dependent thermal responses of UGBG landscapes

The causal effects averaged over the 2001–2020 period reveal substantial differences in how UGBG landscape patterns regulate SUHI across urban scales. Among all landscape metrics, increasing green landscape proportion (G-PLAND) represents the most consistent cooling pathway, producing approximately 1% SUHI reduction across small cities, medium cities, large cities, and megacities. This scale consistency suggests that increasing the relative abundance of green landscapes provides a broadly applicable cooling mechanism under diverse urban contexts. In contrast to landscape quantity, landscape configuration exhibits stronger scale dependence. Increasing green landscape connectivity through G-MESH generates cooling effects across all urban scales, with stronger effects observed in smaller urban systems. This result highlights the importance of spatial organization in determining the thermal benefits of green landscapes, as connected green networks can facilitate continuous ecological processes and enhance landscape-level regulation compared with isolated patches (Bai and Xing, 2025; Liu et al., 2026).

However, fragmentation-related indicators demonstrate contrasting responses between green and blue landscapes. Increased G-PD produces warming effects, consistent with previous findings that excessive fragmentation reduces ecological continuity and weakens landscape-level cooling processes (Bowler et al., 2010; Greene and Kedron, 2018). Conversely, B-PD exhibits cooling effects in larger urban areas, suggesting that the thermal role of fragmentation differs between landscape types. This contrast indicates that landscape configuration metrics cannot be interpreted independently from landscape category, because identical spatial pattern changes may generate different thermal consequences depending on whether they occur in vegetated or aquatic systems.

Landscape shape complexity represents the strongest scale-dependent response among all indicators. GBG-SHAPE shows increasing warming effects with urban scale, while G-SHAPE changes from cooling effects in small and medium cities to warming effects in large cities and megacities. This directional transition suggests that the thermal implications of landscape complexity are not universally positive or negative but depend strongly on urban spatial context. In smaller cities, increased shape complexity may contribute to beneficial edge interactions, whereas in highly urbanized areas, excessive edge effects and fragmented spatial structures may amplify thermal exposure (Qu et al., 2025; Liu et al., 2026; Ren et al., 2026). Therefore, landscape shape optimization requires scale-specific consideration rather than uniform application across cities.

4.2 Temporal dynamics and adaptive implications of UGBG landscape optimization

he temporal analysis further demonstrates that the causal effects of UGBG landscape patterns are dynamic rather than constant throughout urban development. Although SUHI intensity increased during 2001–2020, different landscape indicators exhibited distinct temporal trajectories. G-PLAND maintained a relatively stable cooling effect across all urban scales, indicating that increasing green landscape proportion provides a consistent mitigation pathway throughout different development periods, which is consistent with previous findings on the cooling benefits of urban vegetation (Bowler et al., 2010; Gunawardena et al., 2017). Meanwhile, G-MESH maintained cooling effects across different urban scales, indicating that restoring or enhancing green landscape connectivity can still provide significant thermal benefits throughout the urban development process. (Beele et al., 2024).

In contrast, SHAPE-related indicators showed increasingly divergent temporal responses among urban scales. The warming effects of GBG-SHAPE and G-SHAPE intensified over time in large cities and megacities, whereas smaller cities maintained different or opposite responses. This temporal divergence indicates that the thermal impacts of landscape complexity are strongly dependent on urban development stages and landscape contexts, consistent with previous studies highlighting nonlinear and heterogeneous relationships between urban morphology and thermal environments (Qu et al., 2025; Ren et al., 2026).

Overall, the temporal results indicate that UGBG optimization strategies should consider not only current causal effects but also their long-term evolution. Maintaining sufficient green landscape proportion provides a stable cooling pathway, while improving green landscape connectivity can provide additional cooling benefits, particularly in small and medium cities. However, the thermal effects of landscape complexity require careful consideration of urban scale and future development trajectories.

4.3 Limitations and prospects

Although this study integrates UGBG landscape pattern analysis with causal forest modelling to quantify the causal effects of landscape interventions on SUHI, several limitations remain. First, spatial dependence and potential spillover effects among urban areas may influence causal estimation, as neighboring cities can share similar climatic and landscape characteristics. Future studies could incorporate spatio-temporal causal models to better account for spatial interactions (Christiansen et al., 2022; Runge et al., 2023). Second, although climatic, topographic, and human activity variables were included as controls, potential unobserved confounders, such as planning policies and socio-economic factors, may still exist. Sensitivity analyses and more robust causal approaches could further evaluate the influence of unmeasured factors (Chernozhukov et al., 2018; Zhang et al., 2026). Third, the annual-scale landscape data used in this study cannot fully capture seasonal variations and lagged thermal responses of UGBG landscapes. Future research should integrate higher-temporal-resolution observations to investigate dynamic interactions between UGBG landscape and urban thermal environment (Allen et al., 2021). Fourth, the relatively limited number of megacity samples may introduce uncertainty in scale-specific estimates, requiring validation with additional high-resolution urban datasets. Finally, this study assumes relatively stable causal relationships during 2001–2020, whereas rapid urban transitions may alter SUHI responses to UGBG landscape over time. Future studies could further explore time-varying causal effects under different climate and urban development scenarios.

5 Conclusion

This study developed a causal machine learning framework to quantify the spatiotemporal causal effects of urban green–blue–gray (UGBG) landscape pattern changes on surface urban heat island (SUHI) intensity across 836 urban core units in China from 2001 to 2020. The research revealed how the effects of landscape composition and configuration vary across urban scales and temporal periods. The main conclusions are summarized as follows:

(1) SUHI intensity exhibited a clear urban-scale gradient during 2001–2020. As city scale increased from small cities to megacities, the warming trend of SUHI accelerated, with the Sen's slope increasing from 0.023 to 0.038 °C yr^{-1}. Meanwhile, the mean SUHI intensity increased substantially across all urban scales, with megacities experiencing an increase exceeding 1.5 °C during the study period. These results demonstrate that larger urban systems experienced stronger and faster thermal intensification under continuous urban development.

(2) Green landscape proportion (G-PLAND) represented the most consistent cooling pathway across different urban scales and temporal periods. A 1% increase in G-PLAND generated approximately 1% SUHI reduction in small cities, medium cities, large cities, and megacities, and this cooling effect remained relatively stable from 2001 to 2020. This finding indicates that increasing green landscape proportion provides a broadly applicable strategy for SUHI mitigation across diverse urban contexts.

(3) Landscape connectivity and fragmentation showed scale- and landscape-type-dependent thermal effects. Increasing green landscape connectivity (G-MESH) produced cooling effects across all urban scales, with stronger cooling responses in small and medium cities. These results indicate that connectivity enhancement represents an effective strategy for improving the thermal regulation capacity of urban green landscapes. In contrast, patch density exhibited contrasting effects between landscape types, as increased green landscape fragmentation weakened cooling effects, whereas blue landscape fragmentation showed cooling benefits in larger urban areas. These results demonstrate that configuration metrics should be interpreted jointly with landscape types when evaluating the thermal consequences of landscape pattern changes.

(4) Landscape shape complexity (SHAPE) showed the strongest scale-dependent and temporal variations among all landscape indicators. Increasing GBG-SHAPE produced stronger warming effects with increasing urban scale, while G-SHAPE shifted from cooling effects in small and medium cities to warming effects in large cities and megacities. Moreover, the warming effects of SHAPE-related indicators intensified over time in highly urbanized areas, indicating that the thermal consequences of landscape complexity evolve differently across urban development stages.

(5) The findings demonstrate that effective UGBG optimization requires consideration of both current causal effects and their temporal evolution. Increasing green landscape proportion provides a stable cooling pathway across all urban scales; improving green landscape connectivity can provide additional cooling benefits, particularly in small and medium cities; By revealing the heterogeneous causal effects of landscape pattern changes on SUHI, this study provides scientific evidence for adaptive UGBG planning and contributes to the development of evidence-based strategies for urban heat mitigation under future urbanization.

References

Ahrens, A., Chernozhukov, V., Hansen, C., et al. (2025). An introduction to double/debiased machine learning. arXiv:2504.08324.

Akinnawo, S. O. (2023). Eutrophication: causes, consequences, physical, chemical and biological techniques for mitigation strategies. Environmental Challenges, 12, 100733.

Aleksandrowicz, O., & Pearlmutter, D. (2023). The significance of shade provision in reducing street-level summer heat stress in a hot Mediterranean climate. Landscape and Urban Planning, 229, 104588.

Allen, M. A., Roberts, D. A., & McFadden, J. P. (2021). Reduced urban green cover and daytime cooling capacity during the 2012–2016 California drought. Urban Climate, 36, 100768.

An, Z., Ming, Y., Liu, Y., & Zhang, G. (2025). Investigating 2D/3D factors influencing surface urban heat islands in mountainous cities using explainable machine learning. Urban Climate, 59, 102325.

Araújo, G. R. G., Frassoni, A., & Sapucci, L. F. (2026). Synergistic effects of heatwaves on the surface urban heat island in the São Paulo metropolitan region. Urban Climate, 62, 102998. https://doi.org/10.1016/j.uclim.2026.102998.

Athey, S., Tibshirani, J., & Wager, S. (2019). Generalized random forests. The Annals of Statistics, 47(2), 1179–1203.

Bai, Y., & Xing, Y. (2025). Harnessing green infrastructure for urban heat island mitigation: Evidence-based strategies for sustainable and climate-resilient cities. Sustainable Cities and Society, 128, 106843. https://doi.org/10.1016/j.scs.2025.106843.

Banerjee, S., Yik, S. K., Dzyuban, Y., Crank, P. J., Yi, R. P. X., & Chow, W. T. (2022). Analysing impacts of urban morphological variables and density on outdoor microclimate for tropical cities. Building and Environment, 225, 109646.

Barsi, J. A., Barker, J. L., & Schott, J. R. (2003). An atmospheric correction parameter calculator for a single thermal band earth-sensing instrument. In Proceedings of IEEE IGARSS 2003 (pp. 2–4). IEEE.

Beck, H. E., Zimmermann, N. E., McVicar, T. R., Vergopolan, N., Berg, A., & Wood, E. F. (2020). Present and future Köppen-Geiger climate classification maps at 1-km resolution. Scientific Data, 7(1), 274.

Beele, E., Aerts, R., Reyniers, M., & Somers, B. (2024). Spatial configuration of green space matters: Associations between urban land cover and air temperature. Landscape and Urban Planning, 249, 105121.

Bowler, D. E., Buyung-Ali, L., Knight, T. M., & Pullin, A. S. (2010). Urban greening to cool towns and cities: A systematic review of the empirical evidence. Landscape and Urban Planning, 97(3), 147–155.

Breiman, L. (2001). Random forests. Machine Learning, 45, 5–32.

Cao, W., Zhou, W., Yu, W., & Wu, T. (2024). Combined effects of urban forests on land surface temperature and PM2.5 pollution in the winter and summer. Sustainable Cities and Society, 104, 105309.

Cepeda-Carrion, G., Cegarra-Navarro, J. G., & Cillo, V. (2019). Tips to use partial least squares structural equation modelling (PLS-SEM) in knowledge management. Journal of Knowledge Management, 23(1), 67–89.

Chen, T., & Guestrin, C. (2016). XGBoost: a scalable tree boosting system. In Proceedings of the 22nd ACM SIGKDD International Conference on Knowledge Discovery and Data Mining (pp. 785–794). ACM.

Chen, X. L., Zhao, H. M., Li, P. X., & Yin, Z. Y. (2006). Remote sensing image-based analysis of the relationship between urban heat island and land use/cover changes. Remote Sensing of Environment, 104(2), 133–146.

Chen, X., Zhao, P., Hu, Y., Ouyang, L., Zhu, L., & Ni, G. (2019). Canopy transpiration and its cooling effect of three urban tree species in a subtropical city – Guangzhou, China. Urban Forestry & Urban Greening, 43, 126368.

Chernozhukov, V., Chetverikov, D., Demirer, M., Duflo, E., Hansen, C., Newey, W., & Robins, J. (2018). Double/debiased machine learning for treatment and structural parameters. The Econometrics Journal, 21(1), C1–C68.

Christiansen, R., Baumann, M., Kuemmerle, T., Mahecha, M. D., & Peters, J. (2022). Toward causal inference for spatio-temporal data: conflict and forest loss in Colombia. Journal of the American Statistical Association, 117(538), 591–601.

Credit, K., & Lehnert, M. (2024). A structured comparison of causal machine learning methods to assess heterogeneous treatment effects in spatial data. Journal of Geographical Systems, 26, 483–510.

Cui, P., Xu, D., Tang, J., Lu, J., & Wu, Y. (2024). Assessing the effects of urban green spaces metrics and spatial structure on LST and carbon sinks in Harbin. Sustainable Cities and Society, 113, 105659.

Das, M., Das, A., Rajjack, A., & Singha, S. (2025). Understanding the seasonal pattern and factors affecting cooling effect of blue spaces. Sustainable Cities and Society, 130, 106656.

Du, H. L., Zhan, W. F., Liu, Z. H., Li, J. F., Li, L., Lai, J. M., Miao, S. Q., Huang, F., Wang, C. G., Wang, C. L., Fu, H. Y., Jiang, L., Hong, F. L., & Jiang, S. D. (2021). Simultaneous investigation of surface and canopy urban heat islands over global cities. ISPRS Journal of Photogrammetry and Remote Sensing, 181, 67–83.

Eigenbrod, F., Alexander, P., Apfel, N., Athanasiadis, I. N., Berger, T., Bullock, J. M., Duveiller, G., Equihua, J., Menezes, I., Moreira, R., Paudel, D., Sitokonstantinou, V., Reichstein, M., Willcock, S., & Woodman, T. (2026). Causal machine learning methods for understanding land use and land cover change. Landscape Ecology, 41, 25.

Fei, F., Wang, Y., Yao, W., Gao, W., & Wang, L. (2022). Coupling mechanism of water and greenery on summer thermal environment of waterfront space in China's cold regions. Building and Environment, 214, 108912.

Ferraro, P. J., Sanchirico, J. N., & Smith, M. D. (2019). Causal inference in coupled human and natural systems. Proceedings of the National Academy of Sciences of the United States of America, 116(12), 5311–5318.

Giannarakis, G., Sitokonstantinou, V., Lorilla, R. S., & Kontoes, C. (2022). Towards assessing agricultural land suitability with causal machine learning. arXiv:2408.13155.

Gong, P., Liang, S., Carlton, E. J., Jiang, Q., Wu, J., Wang, L., & Remais, J. V. (2012). Urbanisation and health in China. The Lancet, 379(9818), 843–852.

Greene, C. S., & Kedron, P. J. (2018). Beyond fractional coverage: A multilevel approach to analyzing the impact of urban tree canopy structure on surface urban heat islands. Applied Geography, 95, 45–53.

Grimm, N. B., Faeth, S. H., Golubiewski, N. E., Redman, C. L., Wu, J., Bai, X., & Briggs, J. M. (2008). Global change and the ecology of cities. Science, 319(5864), 756–760.

Gunawardena, K. R., Wells, M. J., & Kershaw, T. (2017). Utilising green and bluespace to mitigate urban heat island intensity. Science of the Total Environment, 584–585, 1040–1055.

Guo, A., Yue, W., Yang, J., He, T., Zhang, M., & Li, M. (2022). Divergent impact of urban 2D/3D morphology on thermal environment along urban gradients. Urban Climate, 45, 101278.

Hamada, S., & Ohta, T. (2010). Seasonal variations in the cooling effect of urban green areas on surrounding urban areas. Urban Forestry and Urban Greening, 9(1), 15–24.

Hathway, E. A., & Sharples, S. (2012). The interaction of rivers and urban form in mitigating the Urban Heat Island effect: A UK case study. Building and Environment, 58, 14–22.

He, J., Shi, Y., Xu, L., Lu, Z., & Feng, M. (2024a). An investigation on the impact of blue and green spatial pattern alterations on the urban thermal environment: A case study of Shanghai. Ecological Indicators, 158, 111244.

He, J., Shi, Y., Xu, L., Lu, Z., Feng, M., Tang, J., & Guo, X. (2024b). Exploring the scale effect of urban thermal environment through XGBoost model. Sustainable Cities and Society, 114, 105763.

Li, S., Leitão, J. P., Wang, Z., & Bach, P. M. (2026). Benefits of pre-screening on more efficient multi-objective optimization of blue-green and grey infrastructures for urban stormwater management. Journal of Environmental Management, 391, 130176. https://doi.org/10.1016/j.jenvman.2026.130176.

Liu, H., Wang, J., Song, J., Przybysz, A., Chen, Y., Song, J., Ma, H., An, W., & Zhu, C. (2026). Nonlinear mechanism of multi-stressors interactions on thermal mitigation efficacy of urban blue-green infrastructure. Sustainable Cities and Society, 107506. https://doi.org/10.1016/j.scs.2026.107506.

Liu, L., Xu, S., Tang, J., Chen, J., et al. (2022). KGML-ag: a modeling framework of knowledge-guided machine learning to simulate agroecosystems. Geoscientific Model Development, 15, 2839–2858.

Liu, X., Wei, M., Li, Z., & Zeng, J. (2016). Landscape pattern changes of urban green space and their ecological impacts. Landscape Ecology, 31, 1591–1604.

Luber, G., & McGeehin, M. (2008). Climate change and extreme heat events. American Journal of Preventive Medicine, 35(5), 429–435.

Magliocca, N. R., Dhungana, P., & Sink, C. D. (2023). Review of counterfactual land change modeling for causal inference in land system science. Journal of Land Use Science, 18(1), 1–24.

Mu, H., Li, X., Wen, Y., et al. (2022). A global record of annual terrestrial Human Footprint dataset from 2000 to 2018. *Scientific Data*, 9, 176. https://doi.org/10.1038/s41597-022-01284-8

Pearl, J. (2000). Causality: Models, reasoning, and inference. Cambridge University Press.

Peng, S., Piao, S., Ciais, P., Friedlingstein, P., Ottle, C., Bréon, F. M., Nan, H., Zhou, L., & Myneni, R. B. (2012). Surface urban heat island across 419 global big cities. Environmental Science & Technology, 46(2), 696–703.

Qu, C., Xu, J., Li, W., Shi, S., & Liu, B. (2025). Quantifying the nonlinear effects of urban-rural blue-green landscape combination patterns on the trade-off between carbon sinks and surface temperature. Sustainable Cities and Society, 128, 106608. https://doi.org/10.1016/j.scs.2025.106608.

Ren, Y., Wen, J., Feng, J., Wang, X., Wang, H., Xie, B., Zhang, C., & Wang, Q. (2026). The non-linear and indirect impacts of urban features on urban Heat Island intensity. Urban Climate, 61, 102986. https://doi.org/10.1016/j.uclim.2026.102986.

Rubin, D. B. (2005). Causal inference using potential outcomes. Journal of the American Statistical Association, 100(469), 322–331.

Runge, J., Gerhardus, A., Varando, G., et al. (2023). Causal inference for time series. Nature Reviews Earth & Environment, 4, 487–505.

Sadeqi, A., & Tabari, H. (2024). Urbanization and climate change implications on cooling demand. Sustainable Cities and Society, 106, 105392.

Sitokonstantinou, V., Porras, E. D. S., Bautista, J. C., et al. (2024). Causal machine learning for sustainable agroecosystems. arXiv:2408.13155.

Sun, R. (2017). How long does the urban heat island effect last? A 10-year observational study. Environmental Research Letters, 12(5), 054012.

Wager, S., & Athey, S. (2018). Estimation and inference of heterogeneous treatment effects using random forests. Journal of the American Statistical Association, 113(523), 1228–1242.

Wu, S., Wang, Y., & Wei, Y. (2026). Evaluation of urban heat island effects based on a three-tier ecological integration network of heating and cooling sources. Energy and Buildings, 117572. https://doi.org/10.1016/j.enbuild.2026.117572.

Yang, J., & Huang, X. (2023). The 30 m annual land cover datasets and its dynamics in China from 1985 to 2022. Earth System Science Data, 13(1), 3907–3925.

Yang, Q., Xu, Y., Chakraborty, T. C., Du, M., Hu, T., Zhang, L., Liu, Y., Yao, R., Yang, J., Chen, S., Xiao, C., Liu, R., Zhang, M., & Chen, R. (2024). A global urban heat island intensity dataset: Generation, comparison, and analysis. Remote Sensing of Environment, 312, 114343.

Zhang, H., Li, Y., Li, M., Wei, S., & Zhang, H. (2026). Explainable and causal machine learning to investigate the spatiotemporal dynamics patterns of coastal water quality in Hong Kong. Water Research, 290, 125026. https://doi.org/10.1016/j.watres.2025.125026.

Zheng, Y., Xu, S., Zhou, C., Wu, Z., & Yang, Y. (2026). Spatial heterogeneity of driving factors for urban heat islands and carbon emissions: Decoding priorities, thresholds, and synergistic interactions. Sustainable Cities and Society, 107518. https://doi.org/10.1016/j.scs.2026.107518.